Failure Analysis of CFRP Tubes with Integrated Rubber Layers Subjected to Transverse Low-Velocity Impact Loading

E. Stelldinger, A. Kühhorn, M. Kober

BTU Cottbus–Senftenberg, Chair of Structural Mechanics and Vehicle Vibration Technology, Siemens-Halske-Ring 14, 03046 Cottbus, Germany

Abstract*: Among the numerous advantages of CFRP laminated structures there are some drawbacks, such as the high sensitivity in terms of impact loading. Particularly low-velocity impacts result in non-visible and barely-visible impact damage respectively. The three-dimensional state of stress in the impact zone leads to matrix cracking and delamination inside the composite laminate and possibly to fibre failure for higher impact energies. It can be very difficult to detect such damage by visual inspection, and additionally, in most cases a significant reduction of strength and stiffness can be expected. To improve the damage tolerance a rubber layer, named KRAIBON®, is integrated in the composite layup of cylindrical carbon/epoxy tubular specimens. Numerous low-velocity impact tests, using different rubber compounds and layups, are carried out. The degree of damage is examined using microsectioning. A reliable prediction of the initiation and propagation of failure, caused by impact loading, requires suitable failure criteria such as the theories of Puck, Cuntze or the LaRC05 criterion. Within this work a theory for initial and progressive failure, based on the Puck failure criterion, is implemented in Abaqus/Explicit using a user material subroutine (VUMAT). The initiation and propagation of interface delamination is modelled using cohesive layer elements. A constitutive hyperelastic material law provided by Abaqus is used to model the constitutive behaviour of the rubber by fitting the hyperelastic constants to experimental test data. The numerical predictions of the local pattern of damage and the impactor reaction force histories, computed by explicit finite element calculations, have been compared with the experimental results.*

Keywords*: Composites, Delamination, Failure, Impact*

1. Introduction

The continuously increasing use of CFRP structures in many industrial branches promotes the development of new failure criteria and also the enhancement of existing theories. The aim is to be able to describe the material behaviour under all possible load conditions. In view of the fast growing computational power, it is possible to analyze more and more complex structures, but also to implement more extensive failure criteria into finite element analysis software. The driving force for the continuous development and improvement of the simulation tools is the possibility to reduce time-consuming and costly component tests. However, in order to verify the simulation tools, some component tests are indispensable. In particular, the complex damage behaviour of CFRP structures makes the calculation of damage due to impact very difficult. An impact causes concentrated out-of-plane loads, which leads to inter-fibre failure, fibre failure and delaminated areas between the plies. Particularly insidious are damages inside the laminate, which cannot be detected by visual inspections, the so-called barely visible impact damages. Such impact loads can occur in a variety of situations, for example tool drops during maintenance and foreign object impacts like hail or stone chip.

In cycle sport CFRP frames are now used in a large number. Unfortunately, the bicycle frames are exposed to numerous impact loads, such as stone chips. In the worst case this can lead to a non-visible damage within the laminate and a subsequent sudden total failure of the bicycle frame. There are already some efforts to increase the impact resistance of the bicycle frames (Kaiser, 2007). Own experimental studies have shown, that the integration of rubber layers into a CFRP laminate, results in a significant increased impact energy damage threshold. However, an efficient optimization of the impact resistance-enhancing measures only is possible by reliable simulations of the damage behaviour of CFRP laminates. In the present work, a combination of the failure theory of Puck and the cohesive layer technology is used.

2. Rubber-layer integration

In order to improve the impact resistance of a CFRP laminate, a rubber layer (KRAIBON®), with a thickness of 0.5 mm, was integrated. Two different rubber compounds were used and placed at different positions within the laminate. However, for the first numerical simulations presented here only the rubber mixture with the internal name SAA9509/21 was used.

2.1 Constitutive law

For the simulation of the material behaviour of the rubber, a hyperelastic model, using the Ogden strain energy potential

$$U = \sum_{i=1}^{N} \frac{2\mu_i}{\alpha_i} (\bar{\lambda}_1^{\alpha_i} + \bar{\lambda}_2^{\alpha_i} + \bar{\lambda}_3^{\alpha_i} - 3)^i + \sum_{i=1}^{N} \frac{1}{D_i} (J_{el} - 1)^{2i} \text{ ,}$$

with an order of $N = 3$ was applied. Here, $\bar{\lambda}_i$ are the principal deviatoric stretches and J_{el} is the elastic volume strain. The material coefficients μ_i and α_i have been calibrated by Abaqus on the basis of tensile and compressive test data provided by Gummiwerk KRAIBURG. Due to the lack of volumetric compression test data, the Poisson´s ratio has been assumed to be ν = 0.4995. Taking into account the relationship

$$\nu = \frac{3K_0 / \mu_0 - 2}{6K_0 / \mu_0 + 2},$$

the initial shear modulus

$$\mu_0 = \sum_{i=1}^{N} \mu_i$$

and the initial bulk modulus

$$K_0 = \frac{2}{D_1}$$

the value for D_1 is computed as approximately 0.002, by using the parameters listed in Table 1. D_2 and D_3 are set to zero. The verification of the Drucker stability showed a stable behavior of the model for all strains. More details can be found in the Abaqus Users Manual.

Table 1. Ogden material parameters for the rubber compound SAA9509/21.

i	μ_i	α_i	D_i
1	-55.498	4.698	0.002
2	23.930	5.324	0
3	32.575	4.037	0

3. Impact tests

The damage response of laminated composites due to low-velocity impact has been studied experimentally by many authors. Some surveys are published by (Agrawal, 2014; Cantwell, 1991). For the implementation of low-velocity impact tests two common procedures exist: Testing by drop-weight impact towers, which is more commonly used and the use of a pendulum impact tester (charpy pendulum). In the present investigation, a charpy pendulum, equipped with a spherical impactor (D = 15 mm) and a force transducer, was used. The impact energy can be varied by the initial excursion of the pendulum. As test objects tubular specimens with a length of 200 mm and a diameter of 60 mm, made of CFRP and rubber, were used. In most cases, the focus was on the investigation of the damage profiles due to impacts with an impact energy range from E_{imp} = 10 J upwards. The test objects were mostly plates, made of fibre-reinforced plastics (Agrawal, 2014). However, in practical application cases, real components usually have curved surfaces. On the basis of extensive experimental studies (Ehrlich, 2004) showed, that the curvature of the impacted surface, cannot be neglected with respect to the impact behaviour. Another finding was, that structures with convex curved impact surfaces have a significantly greater damage than planar structures. Experimental tests of bicycle frame tubes, made of CFRP, have shown that even impact energies of E_{imp} = 0.5 J cause significant damage within the laminate (Kaiser, 2007). For this reason, three samples were tested for each layup with a relatively small impact energy starting at 0.15 J. Subsequently, the impact energy was increased in 0.15 J steps until a first drop in the load response was evident (see Figure 1).

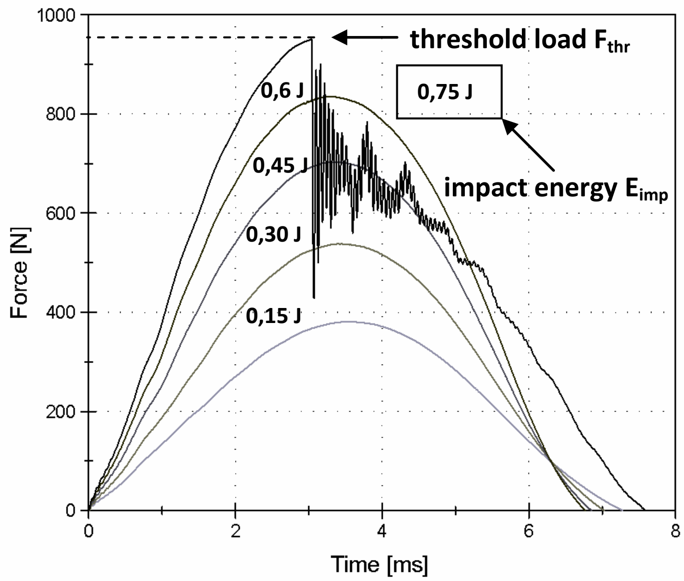

Figure 1. Exemplary force-time histories.

In addition, numerous tests were carried out at higher impact energies and with impact energies just below the determined delamination threshold values. For the investigation of the extent of damage, the specimens were examined by microsectioning. The cross sectional cut runs directly through the point of the initial contact between impactor and specimen. Some of these microsectioning examinations have shown that there are a few inter-fibre failures without any indication in the force-time history. This leads to the conclusion that each drop in the load response is caused by delaminations or fibre failures. For the implementation of the numerical simulations only the reference sample layup and the layup with the best impact performance were selected: Reference: [±45/0_2/±45/0_2/±45]; I1O: [±45/RUBBER/0_2/±45/0_2/±45].

4. Failure models used for numerical investigations

Thanks to the efforts within the framework of the three world wide failure exercises (Hinton, 2004; Kaddour, 2012; Kaddour, 2013), great progress could be achieved in the field of failure analysis of fibre reinforced plastics. In the present work Puck´s model (Puck, 1996; Puck, 1998) has been selected because it was able to achieve very good results in the first and second exercise. This action plane-related failure criterion is physically based on the hypothesis of Coulomb and Mohr and suitable for brittle fracture. In addition, a degradation model has been chosen, which enables a reduction of the stiffness of damaged regions, depending on the result variables of Puck´s approach and the stress conditions in this region. In order to make these models available for Abaqus/Explicit, these theories have been implemented in a user defined material model (VUMAT). As the propagation of delaminations cannot be described with this model, a cohesive layer approach provided by Abaqus/Explicit has been used.

4.1. Fibre failure (FF)

Damage initiation

One of the basic characteristics of Puck´s failure criterion is the distinction between FF and IFF. To predict the fiber breakage an extended fiber fracture criterion has now been established. This formulation involves the fibre perpendicular stresses, which, due to the Poisson´s effect, cause additional stresses in the fibres (Puck, 1998; Puck, 2002; Deuschle; 2012):

$$f_{E\,FF} = \frac{1}{\pm R_{\parallel}^{t,c}} \left[\sigma_1 - \left(\nu_{\perp\parallel} - \nu_{\perp\parallel f} \cdot m_{\sigma f} \frac{E_{\parallel}}{E_{\parallel f}} \right) (\sigma_2 + \sigma_3) \right] \quad \text{with} \quad \begin{cases} R_{\parallel}^{t} & for[...] \geq 0 \\ -R_{\parallel}^{c} & for[...] < 0 \end{cases}$$

If the stress exposure increases to $f_{E\,FF} = 1$, fibre breakage occurs. The magnification factor $m_{\sigma f}$ takes into account the inhomogeneous stress field in the matrix. The transverse stresses are slightly larger near the fibre, so the factor is set to the value $m_{\sigma f} = 1.1$ for CFRP (Deuschle; 2012).

Damage propagation

As soon as fibre breakage occurs, all stiffnesses are degraded to 1% of their initial value.

4.2. Inter - fibre failure (IFF)

Damage initiation

The IFF model of Puck is a very well-proven model and has been used by many authors. For this reason, the explanations have been kept quite short. The basic idea is, that the fracture occurs on a fiber-parallel plane, on which the stress exposure reaches the value of $f_E(\theta) = 1$ at first. For this reason, all acting stresses must be transformed to potential fracture planes in a range of $\theta = [-90°; 90°]$:

$$\sigma_n(\theta) = \sigma_2 \cdot \cos^2\theta + \sigma_3 \cdot \sin^2\theta + 2\tau_{23} \cdot \sin\theta \cdot \cos\theta$$
$$\tau_{nt}(\theta) = -\sigma_2 \cdot \sin\theta \cdot \cos\theta + \sigma_3 \cdot \sin\theta \cdot \cos\theta + \tau_{23} \cdot (\cos^2\theta - \sin^2\theta)$$
$$\tau_{n1}(\theta) = \tau_{31} \cdot \sin\theta + \tau_{21} \cdot \cos\theta$$

An angle of $\theta = 0°$ means that the fracture surface runs perpendicular to the 2-direction. The following two expressions of the stress exposure only depend on these three action plane-related stresses and the fracture resistances related to the action plane:

$$f_{E\ IFF}(\theta) = \sqrt{\left[\left(\frac{1}{R_\perp^{At}} - \frac{p_{\perp\psi}^t}{R_{\perp\psi}^A}\right) \cdot \sigma_n(\theta)\right]^2 + \left(\frac{\tau_{nt}(\theta)}{R_{\perp\perp}^A}\right)^2 + \left(\frac{\tau_{n1}(\theta)}{R_{\perp\parallel}^A}\right)^2} + \frac{p_{\perp\psi}^t}{R_{\perp\psi}^A} \cdot \sigma_n(\theta)$$

for $\sigma_n(\theta) \geq 0$ and

$$f_{E\ IFF}(\theta) = \sqrt{\left(\frac{p_{\perp\psi}^c}{R_{\perp\psi}^A} \cdot \sigma_n(\theta)\right)^2 + \left(\frac{\tau_{nt}(\theta)}{R_{\perp\perp}^A}\right)^2 + \left(\frac{\tau_{n1}(\theta)}{R_{\perp\parallel}^A}\right)^2} + \frac{p_{\perp\psi}^c}{R_{\perp\psi}^A} \cdot \sigma_n(\theta)$$

for $\sigma_n(\theta) < 0$. Here, the following relationships are valid:

$$R_\perp^{At} = R_\perp^t; \quad R_{\perp\parallel}^A = R_{\perp\parallel}; \quad R_{\perp\perp}^A = \frac{R_\perp^c}{2(1 + p_{\perp\perp}^c)};$$

$$\frac{p_{\perp\psi}^{t,c}}{R_{\perp\psi}^A} = \frac{p_{\perp\perp}^{t,c}}{R_{\perp\perp}^A}\cos^2\psi + \frac{p_{\perp\parallel}^{t,c}}{R_{\perp\parallel}^A}\sin^2\psi \quad \text{with} \quad \cos^2\psi = \frac{\tau_{nt}^2}{\tau_{nt}^2 + \tau_{n1}^2}; \quad \sin^2\psi = \frac{\tau_{n1}^2}{\tau_{nt}^2 + \tau_{n1}^2}.$$

In reality, not only the three action plane-related stresses (σ_n, τ_{nt} and τ_{n1}) are relevant for IFF. For this reason, Puck supplemented his theory with two extensions. The first one takes into account the influence of high fibre parallel stresses (σ_1). Due to high stresses in 1-direction some fibres already fail before reaching the strength limit. The results are local micro-fractures and fibre-matrix debonding, which reduces the resistance against IFF. The second extension concerns the influence of non-fracture plane stresses and probabilistic effects in an analytical manner. Both extensions have been integrated into the VUMAT, but should not be discussed in detail here. The definition of all required variables is made according to the recommendations of the authors. Detailed explanations can be found for example in (Deuschle, 2012).

Damage propagation

Numerous studies have shown, that prior to the formation of first macroscopic cracks, a variety of micro cracks leads to a nonlinear material behaviour (Kopp, 1999). However, the consideration of these nonlinearities should be a part of future work. Within the meaning of pucks failure condition, a stress exposure of $f_{E\ IFF} = 1$ leads to first macroscopic cracks. There are already different ways to consider the post-failure behaviour of composite materials. For IFF, continuum damage models, based on the smeared crack approach, are still by far the most widely used. Smeared crack means, that the effects of a discrete crack are evenly distributed over the whole continuum. In context of FEM, the material stiffness must be degraded in the material point where $f_{E\ IFF}$ has reached the value of one. A very simple procedure is the “ply-discount method”, which suddenly degrades the stiffnesses of the ply to the residual stiffnesses. Other possibilities would be, for example, to degrade on the basis of an empirical function (depending on $f_{E\ IFF}$) or the “constant IFF stress exposure approach” (Puck, 2002; Deuschle, 2010). The latter approach was chosen, because this is very simple and yet reasonable. Here, the stress exposure is kept constant at $f_{E\ IFF} = 1$ by the ply stiffness values. The idea behind this is, that when the stress exposure of a layer exceeds the value of 1, immediately another crack occurs and thus reduces the stiffness and the stress exposure, respectively. Micro mechanical studies have shown that the degradation of the individual material parameters (E_2, E_3, G_{12}, G_{13}, G_{23}) should be carried out in dependence of the fracture angle θ_{fp}. In (Deuschle, 2010) the development of an approach for fracture angle-dependent degradation is presented. In (Deuschle, 2012) a simplified version of this approach is used. However, using these approaches for the present problem leads to an unstable damage evolution. The reason is that due to the loads in thickness direction no load redistribution in adjacent layers is possible. Therefore, only the in-plane material parameters (E_2, G_{12},) were degraded, which leads to the following modified degradation rule, following (Deuschle, 2012):

$$E_2^{\deg} = \begin{cases} E_2 \cdot (1-\delta \cdot \cos(\theta_{fp})) & for \quad \sigma_n > 0 \\ E_2 & for \quad \sigma_n \le 0 \end{cases}$$

$$G_{12}^{\deg} = G_{12} \cdot (1-\delta \cdot 0{,}6 \cdot \cos(\theta_{fp}))\,.$$

Where $\delta = [0;0.97]$ is the damage variable. The upper limit of δ was set to $\delta_{max}=0.97$ to ensure a residual E-moduli of 3% (Knops, 2003). Following (Deuschle, 2012) it is assumed, that the G-moduli experience about 0.6 times the reduction of the E-moduli. When IFF occurs, the damage variable δ is gradually increased to maintain a constant $f_{E\ IFF} = 1$, until all stiffnesses have reached their residual stiffness values.

4.3. Delamination

Damage initiation

A delamination is caused by the three stresses, σ_{33}, σ_{13} and τ_{23}, acting on the interface between two layers. Consequently, a delamination initiation criterion should be based on these three stresses. A very good overview of existing delamination failure criteria can be found in (Abrate, 2011). Puck´s action plane-related failure criterion includes the delamination as special case. Thus, a delamination occurs if the stress exposure f_E reaches its maximum value of $f_E = 1$ on an action-plane of $\theta = \pm 90°$.
However, with regard to the damage propagation due to delamination initiation, a suitable theory must be used, which accounts for the stress singularity at the delamination front. Abaqus provides, by the use of cohesive elements, some very powerful displacement and energy based degradation approaches. For this reason, an Abaqus-integrated delamination initiation approach was used. Besides the maximum nominal stress criterion another stress based criterion, the quadratic nominal stress criterion

$$\left\{\frac{\langle t_n \rangle}{t_n^0}\right\}^2 + \left\{\frac{t_s}{t_s^0}\right\}^2 + \left\{\frac{t_t}{t_t^0}\right\}^2 = 1,$$

is provided by Abaqus and used in the present work. For the application of this approach the constitutive response of the cohesive layer has to be defined in terms of a traction-separation law. Where t_n is the nominal traction stress in 3-direction, t_s and t_t in 1- and 2-directions. t_n^0, t_s^0, and t_t^0 are the maximum bearable nominal stresses in the three directions, respectively. Following the recommendations of Puck, the interlaminar strengths must be reduced with an weakening factor of 0.8 ÷ 0,9. The reasons are increased fibre waviness and imperfections in the form of air-entrapping, which on this interfaces are more likely to occur due to fibre crossings (Puck, 1996). The strength values reduced by a factor of 0.8 can be found in Table 3. Under the assumption that the constitutive behaviour is uncoupled, the nominal traction stresses can be calculated as follows

$$\begin{Bmatrix} t_n \\ t_s \\ t_t \end{Bmatrix} = \begin{bmatrix} E_{nn} & 0 & 0 \\ 0 & E_{ss} & 0 \\ 0 & 0 & E_{tt} \end{bmatrix} = \begin{Bmatrix} \varepsilon_n \\ \varepsilon_s \\ \varepsilon_t \end{Bmatrix}$$

Where ε_n, ε_s and ε_t are the nominal strains, which are equal to the separations if the nominal layer thickness is set to T=1. More information can be found in the Abaqus analysis user´s guide.

Damage propagation

The damage propagation is defined in the form of an evolution law based on fracture-energy. To specify the dependence of the fracture energy on the mode mix, the power law form is used:

$$\left\{\frac{G_n}{G_n^C}\right\}^{\alpha} + \left\{\frac{G_s}{G_s^C}\right\}^{\alpha} + \left\{\frac{G_t}{G_t^C}\right\}^{\alpha} = 1.$$

Where G_n^C, G_s^C and G_t^C are the values for the fracture toughness, which refer to the critical fracture energies required to cause failure in the respective direction. The corresponding values are given in Table 3.

4.4 Material properties

For the manufacturing of the tubular specimens the unidirectional prepreg KUBD1507 was used. The corresponding material data, which are used for the numerical simulations, are listed in Table 2 and Table 3.

Table 2. Material data KUBD1507.

Density	ρ = 1556 kg/m³
Elastic properties	E_1 = 121400 MPa*[1]; $E_2 = E_3$ = 7000 MPa; E_{1f} = 234000 MPa $G_{12} = G_{13}$ = 4000 MPa*[2]; G_{23} =3200 MPa*[2] $\nu_{12} = \nu_{13}$ = 0.3*[2]; ν_{23} = 0.4*[2]; $\nu_{\|\perp f}$ = 0.2*[2]
Strengths	$R_{\|}^{t}$ = 1680 MPa*[1]; $R_{\|}^{c}$ = 1200 MPa*[2] $R_{\perp}^{t}$ = 135 MPa; $R_{\perp}^{c}$ = 200 MPa*[2] $R_{\perp\|}$ = 85 MPa
Inclination parameter	$p^{t}_{\perp\|}$ = 0.35*[3]; $p^{c}_{\perp\|}$ = 0.30*[3]; $p^{t}_{\perp\perp} = p^{c}_{\perp\perp}$ = 0.275*[3]

*1 Test data; *2 Assumed; *3 recommendation of the author

Table 3. Material data cohesive layer.

Density	ρ = 1556 kg/m³
Elastic properties	K_{nn} = 7000 MPa; $K_{ss} = K_{tt}$ = 4000 MPa*[2]
Strengths	t^0_n =108 MPa; $t^0_s = t^0_t$ = 65 MPa
Fracture toughness	G_n^C = 0.8 N/mm*[2]; $G_s^C = G_t^C$ = 0.3 N/mm*[2]; α = 1*[2]

*2 Assumed

5. Numerical investigations

The finite element model was created using Abaqus/CAE (see Figure 2). The CFRP tubular specimens have a length of 200 mm and an outer diameter of 60 mm. The tube is supported about half the circumference on the back. The space between the two support elements is 40 mm. The impactor is modelled as a rigid body with a diameter of 15 mm.

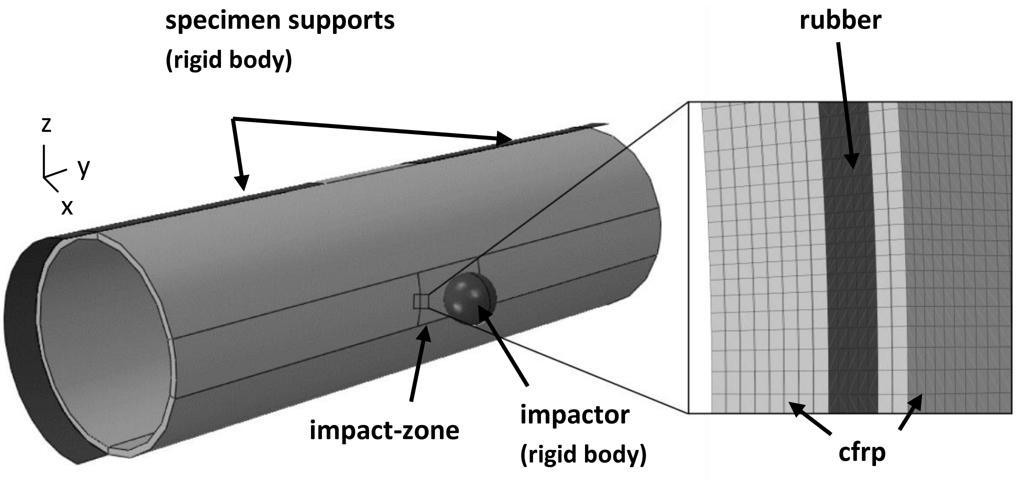

Figure 2. Finite element model

The impactor revolves around an axis in a distance of 382 mm. The inertia about this axis was set to 0,384 kg/m², which is exactly the inertia of the real charpy pendulum. Consequently, the impact energy can be varied by changes in the initial angular velocity. The contact between the different contact surfaces is modelled using the general contact algorithm provided by Abaqus/Explicit. In normal direction a "Hard" contact was defined, while the tangential behaviour is simulated by a penalty formulation using a friction coefficient with a value of $\mu = 0.3$. To reduce the effort due to mesh modifications and associated allocations of the material orientations, the impact-zone (see Figure 2) is modelled as a separate region and tied to the surrounding mesh-region. Some studies for the estimation of errors which are induced by using this approach can be found in (Keskin, 2015). Inside the impact-zone the lateral dimension of the elements is about 0.2 mm up to 1 mm in the edge region. Through the thickness one C3D8R element per laminate ply is used. Each layer has a thickness of 0.14 mm, while the interface has a thickness of 0.01 mm and is discretized with COH3D8 elements. The rubber layer is modelled using four fully integrated elements (C3D8) through the thickness. To prevent hourglass modes of the C3D8R elements the stiffness relaxation hourglass control has been used.

6. Results

6.1. Reference test series

The test results are listed in Table 4, showing a fairly good repeatability of the IR – test series. All initial delaminations have been detected at the same impact energy, within a very narrow range of threshold loads. The accordance of the force-time histories is quite good, but in the simulation, the first delamination already occurs at a contact force of about 580 N (see Figure 5). Accordingly, also the extent of the delaminations is significantly greater in the simulation (see Figure 3 (top) and 4 (top)). Figure 3 (top) shows an example of a cross-section cut of a sample after a 0,3 J – impact. The detected damages are IFF (Mode A) in ply 10 and a delamination at the interface 9-10. In addition a cross-section cut due to a 0.45 J – impact is shown (see Figure 4 (below)).

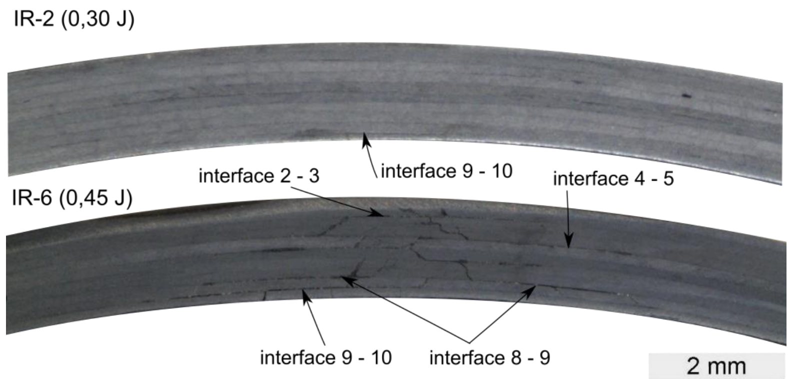

Figure 3. Section cut views: Experiment

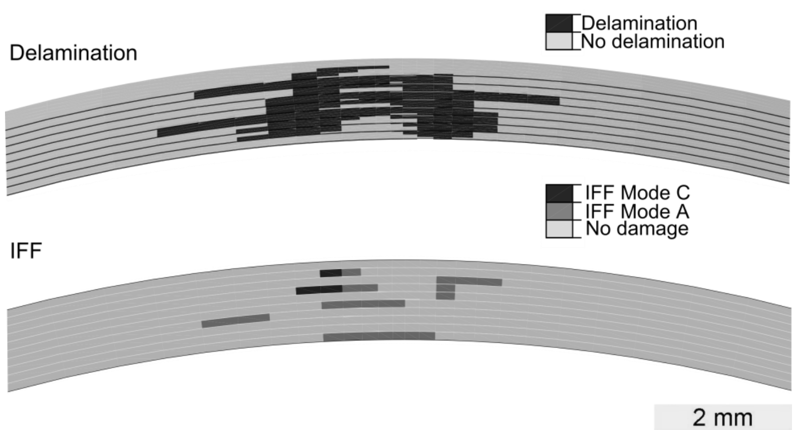

Figure 4. Section cut views: Simulation (IR, 0.30 J)

Table 4. Test results IR* - series.

Specimen name	Impact energy E_{imp} [J]	Threshold load F_{thr} [N]
IR-1	0.30	719
IR-2	0.30	774
IR-3	0.30	707

* [±45 /0_2/±45/0_2/±45]

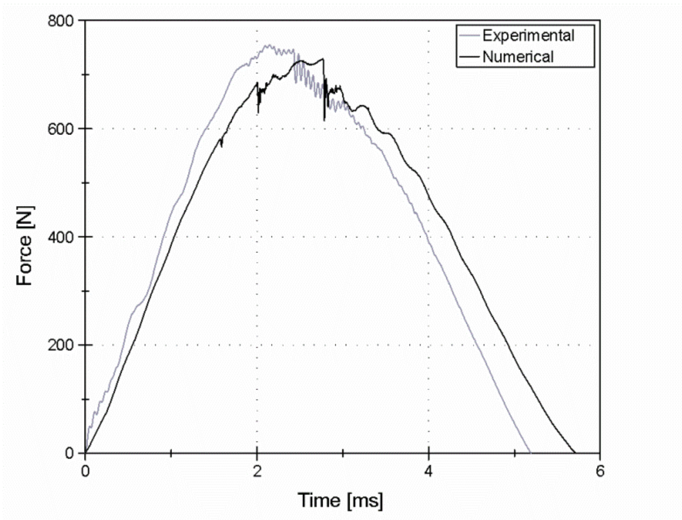

Figure 5. Force vs. time histories of IR-1.

6.2. I1O test series

The impact test series I1O shows with respect to the delamination threshold load a certain scattering (see Table 5). As a result, the respective first delaminations occurred at different impact energies. At a high impact energy, the correspondingly high internal energy at the time of the damage initiation leads to greater damage. The damage in consequence of the impact energy of 0.6 J is only a small delamination at the interface 5-6, while the damage as a result of the 1.35 J – impact has significantly greater proportions (see Figure 6).

Table 5. Test results I1O* - series.

Specimen name	Impact energy E_{imp} [J]	Threshold load F_{thr} [N]
I1O-1	0.75	951
I1O-2	1.35	1090
I1O-3	0.60	836

* [±45/RUBBER/0_2/±45/0_2/±45]

Numerical investigations were carried out at all three impact energies (0.60 J; 0.75 J; 1.35 J). An impact energy of 0.60 J leads to no damage in the numerical simulations. The 0.75 J - impact caused IFF (mode A) located in layer 2 and layer 10, but no delaminations occurred. Finally the 1.35 J - impact simulation led to large delaminations and numerous IFF (mode A and mode C). Figure 8 shows a comparison of the contact force histories due to the 1.35 J – impact. The good agreement of the initial slopes of both curves shows, that the total stiffness can be reproduced very well by the use of the constitutive model, as described in Section 2.1. However, the damage process begins at a slightly higher contact force than predicted in the experiment. In addition, the major delaminations were predicted at the interfaces 7-8 and 8-9, in contrast to the interfaces 8-9 and 9-10 in the experiment. These gaps can be explained by assuming, that the matrix crack tips act as delamination initiation trigger. These stress singularities due to IFF are not considered by the simulation. In the numerical model, the effects of the IFF are taken into account only by some load redistribution to adjacent layers.

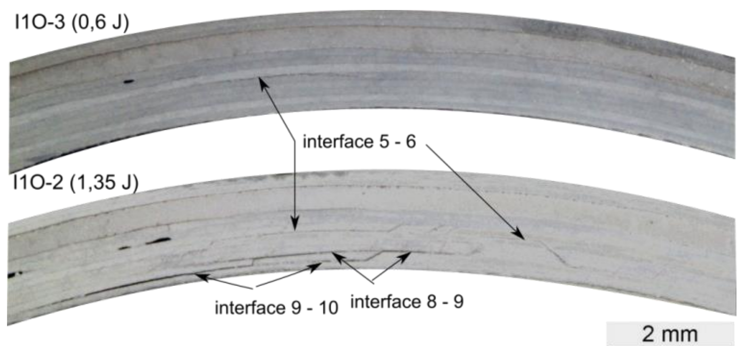

Figure 6. Section cut views (Experiment)

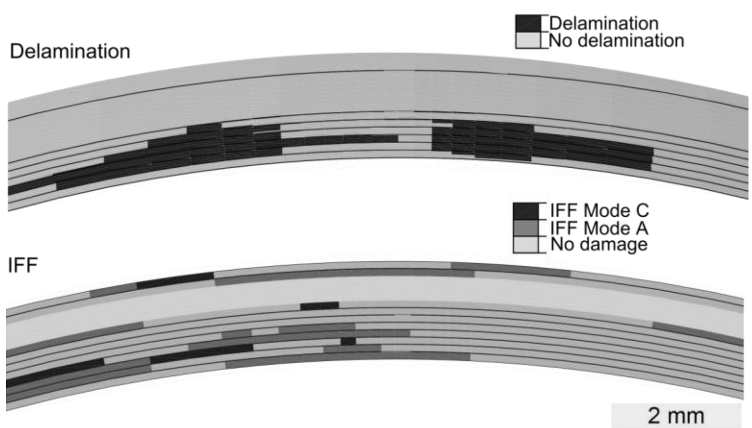

Figure 7. Section cut views: Simulation (I1O, 1.35 J)

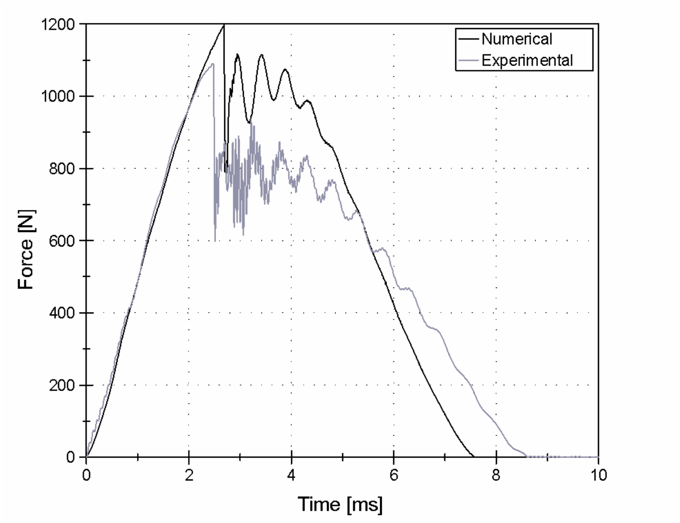

Figure 8. Force vs. time histories of I1O-2

7. Conclusions

The action plane-related failure criterion of Puck, including a suitable degradation model, was implemented using a user defined material subroutine (VUMAT). In addition cohesive layer elements were used for the prediction of delamination initiation and propagation. The results of the numerical simulations show a good accordance to the experimental investigations. The experimentally determined improvement of impact tolerance by integrating a rubber layer (*KRAIBON®)*, could be reproduced by the numerical simulations. The good agreement of the numerical and experimental force-time histories of the I1O - test series show, that the material behaviour of the rubber was very well captured by the hyperelastic material law. This opens up the possibility to optimize parameters such as rubber compound, rubber layer thickness and stacking sequence in terms of an impact resistance improvement.

8. References

1. Abrate, S., „Impact Engineering of Composite Structures“, SpringerWienNewYork, 2011.

2. Agrawal, S., Singh, K. K., Sarkar, P. K., “Impact Damage on Fibre-Reinforced Polymer Matrix Composite – A Review”, no. 48, pp. 317-332, 2014.

3. Cantwell W., Morton J., “The Impact Resistance of Composite Materials – A Review”, Composites, no. 22, pp. 347–362, 1991.

4. Deuschle, H. M., „ 3D Failure Analysis of UD Fibre Reinforced Composites: Puck´s Theory within FEA”, Thesis, Universität Stuttgart, 2010.

5. Deuschle, H. M., Kröplin, B. H., „ Finite Element Implementation of Puck´s Failure Theory for Fibre-Reinforced Composites under Three-Dimensional Stress”, Journal of Composite Materials, no. 46, pp. 2485-2513, 2012.

6. Ehrlich, I., “Impactverhalten schwach gekrümmter Strukturen aus faserverstärkten Kunststoffen”, Dissertation, Universität der Bundeswehr München, 2004.

7. Hinton, M.J., Kaddour, A.S., and Soden, P.D. “Failure Criteria in Fibre Reinforced Polymer Composites: The World-Wide Failure Exercise, Elsevier, 2004.

8. Kaddour, A. S., and Hinton, M. J., “Benchmarking of Triaxial Failure Criteria for Composite Laminates: Comparison between Models of ‘Part (A)’ of ‘WWFE-II’”, Journal of Composite Materials, no. 46, pp. 2595–2634, 2012.

9. Kaddour, A. S., Hinton, M. J, Smith, P. A., and Li, S., “The Background to the Third World-Wide Failure Exercise”, Journal of Composite Materials, pp. 2417-2426, 2013.

10. Kaiser, M., “Zur Anwendung von kohlenstofffaserverstärktem Konststoff im Hochleistungs-Rahmenbau von Sporträdern”, Dissertation, Technische Universität Kaiserslautern, 2007.

11. Keskin, A., et al. “On The Quantification of Errors of a Pre-Processing Effort Reducing Contact Meshing Approach” , AIAA SciTech 2015, Kissimmee, Florida, 5 - 9 January 2015.

12. Knops, M., “Sukzessives Bruchgeschehen in Faserverbundlaminaten”, Dissertation, RWTH-Aachen, 2003.

13. Kopp, J. W., “Zur Spannungs- und Festigkeitsanalyse von unidirektionalen Faserverbundkuststoffen”, Dissertation, RWTH-Aachen, 1999.

14. Puck, A.,”Festigkeitsanalyse von Faser-Matrix-Laminaten, Modelle für die Praxis“, Carl-Hanser-Verlag, München, 1996.

15. Puck, A., and Schürmann, H., „Failure Analysis of FRP Laminates by Means of Physically Based Phenomenological Models“, Composites Science and Technology, pp. 1045-1067, 1998.

16. Abaqus Users Manual, Version 6.13, Dassault Systémes Simulia Corp., Providence, RI.